

## Research Article

# Experimental Investigation of $\text{CaMnO}_{3-\delta}$ Based Oxygen Carriers Used in Continuous Chemical-Looping Combustion

Peter Hallberg,<sup>1</sup> Malin Källén,<sup>1</sup> Dazheng Jing,<sup>2</sup> Frans Snijkers,<sup>3</sup>  
Jasper van Noyen,<sup>3</sup> Magnus Rydén,<sup>1</sup> and Anders Lyngfelt<sup>1</sup>

<sup>1</sup> Department of Energy and Environment, Chalmers University of Technology, 412 96 Gothenburg, Sweden

<sup>2</sup> Department of Inorganic Environmental Chemistry, Chalmers University of Technology, 412 96 Gothenburg, Sweden

<sup>3</sup> Flemish Institute for Technological Research (VITO), 2400 Mol, Belgium

Correspondence should be addressed to Peter Hallberg; [peter.hallberg@chalmers.se](mailto:peter.hallberg@chalmers.se)

Received 11 December 2013; Revised 24 March 2014; Accepted 5 April 2014; Published 12 June 2014

Academic Editor: Jerzy Bałdyga

Copyright © 2014 Peter Hallberg et al. This is an open access article distributed under the Creative Commons Attribution License, which permits unrestricted use, distribution, and reproduction in any medium, provided the original work is properly cited.

Three materials of perovskite structure,  $\text{CaMn}_{1-x}\text{M}_x\text{O}_{3-\delta}$  ( $\text{M} = \text{Mg}$  or  $\text{Mg}$  and  $\text{Ti}$ ), have been examined as oxygen carriers in continuous operation of chemical-looping combustion (CLC) in a circulating fluidized bed system with the designed fuel power 300 W. Natural gas was used as fuel. All three materials were capable of completely converting the fuel to carbon dioxide and water at 900°C. All materials also showed the ability to release gas phase oxygen when fluidized by inert gas at elevated temperature (700–950°C); that is, they were suitable for chemical looping with oxygen uncoupling (CLOU). Both fuel conversion and oxygen release improved with temperature. All three materials also showed good mechanical integrity, as the fraction of fines collected during experiments was small. These results indicate that the materials are promising oxygen carriers for chemical-looping combustion.

## 1. Introduction

Combustion of fossil fuels results in increased concentration of the greenhouse gas  $\text{CO}_2$  in the atmosphere. As the global consumption of fossil fuels continues to increase, limiting global warming to the internationally agreed upon target 2°C [1] will be difficult. All possible tools will likely be needed if this effort is to be successful. One such mitigation tool is carbon capture and storage (CCS) [2]. The basic idea with CCS is to capture the  $\text{CO}_2$  from large emission sources, for example, fossil fueled power plants and industrial processes. The captured  $\text{CO}_2$  can then be compressed and transported to a storage site, which can be, for example, a deep saline aquifer or a depleted natural gas field. With CCS fossil fuels can be utilized without contributing to anthropogenic climate change. There are various ways to separate  $\text{CO}_2$  from other flue gases and they typically come with a significant energy penalty [2].

## 2. Background

**2.1. Chemical-Looping Combustion.** Chemical-looping combustion (CLC) is a fuel oxidation process with inherent  $\text{CO}_2$  separation. In CLC oxygen is provided to the fuel with a solid oxygen carrier, which is usually a metal oxide ( $\text{Me}_x\text{O}_y$ ). A system where the oxygen carrier is continuously circulated between two reactors has been successfully tested in different scales [3–6]. Several reviews of chemical-looping combustion research and development have been made in the last years [7–9]. A schematic image of the general principle is shown in Figure 1.

In the fuel reactor (FR) the fuel is oxidized by the oxygen carrier, according to reaction (1). The flue gases consist of mainly  $\text{CO}_2$  and steam. Steam is easily condensed so that almost pure  $\text{CO}_2$  remains. So by preventing dilution of the flue gases with nitrogen from the air no energy consuming gas separation is needed to obtain  $\text{CO}_2$  of sufficiently high

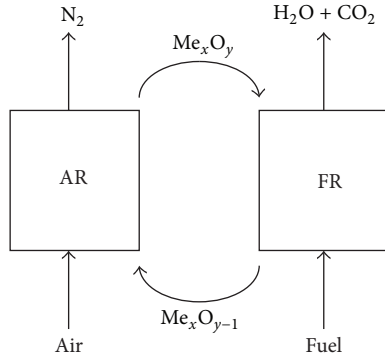
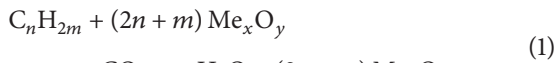
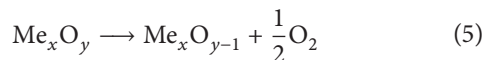


FIGURE 1: A schematic picture of the CLC process.

purity for transport and storage. This makes CLC an almost ideal technology for CCS. Another important advantage over conventional combustion is that due to the relatively low temperature used, typically around 1000°C, thermal NO<sub>x</sub> formation is avoided [10]. After the fuel oxidation, the oxygen depleted oxygen carrier is circulated to the air reactor (AR) to be reoxidized with air, according to reaction (2). Consider



Note that the sum of reactions (1) and (2) is identical to conventional combustion and thus the heat output from CLC is the same as conventional combustion. Reaction (1) is typically considered as a gas-solid reaction. So when the fuel is a solid, such as coal or biomass char, an intermediate step is needed where the char is gasified. This can be done according to reaction (3) or reaction (4) using steam or CO<sub>2</sub> as reagent. However, if the oxygen carrier is chosen so that oxygen in gas phase is released spontaneously at FR conditions (high temperature, low oxygen partial pressure) this intermediate step is not needed. This concept with gas phase oxygen release from the oxygen carrier is called chemical looping with oxygen uncoupling (CLOU) [11] and is described by reaction (5). Consider



Oxygen released via reaction (5) will react with char in an ordinary combustion reaction without diluting the flue gas with nitrogen and the reduced oxygen carrier can be reoxidized in the air reactor via reaction (2). The sum of reactions (3)-(4) can be avoided. This makes CLOU an attractive concept mainly for oxidation of solid fuels.

CLOU is also highly interesting for gaseous fuels application as well since it has the potential to improve fuel conversion by providing oxygen for gas-gas reaction, in addition to the gas-solid reaction between fuel and oxygen carrier.

**2.2. Oxygen Carriers of Perovskite Structure.** The ability of an oxygen carrier to release gas phase oxygen in the chemical looping fuel reactor is dictated by its thermodynamic properties. Metal oxides which are suitable for CLOU include CuO, Mn<sub>2</sub>O<sub>3</sub>, and various combined oxides such as (Mn, Fe)<sub>2</sub>O<sub>3</sub> [2, 12]. Another option which has been examined is CaMnO<sub>3-δ</sub> which is a material of perovskite structure. A material of perovskite structure has the general formula ABC<sub>3-δ</sub>, where A and B are a large cation and a small cation, respectively, C is usually oxygen, and in that case δ expresses the oxygen deficiency in the structure. A or B does not have to be a single ion but combinations of ions of similar size and oxidation state are possible. For the use as oxygen carrier other alternatives than manganese for the B site are iron, titanium, and possibly copper, nickel, or cobalt. For the A site calcium seems to be the best candidate although lanthanum and strontium are other possibilities. The formability of materials of perovskite structure has been extensively investigated by Li et al. [13] What makes perovskites interesting for chemical-looping combustion is that the oxygen deficiency δ is a function of the surroundings; that is, it changes depending on factors such as temperature, pressure, and ambient partial pressure of oxygen. In the fuel reactor with low oxygen partial pressure δ would increase, thus releasing oxygen, whereas it would decrease in the air reactor with comparatively high oxygen partial pressure. These changes do not necessarily occur at conditions relevant for chemical-looping combustion for all perovskite materials, but in CaMnO<sub>3-δ</sub> they do. Alas, Bakken et al. have shown that CaMnO<sub>3-δ</sub> decomposes to Ca<sub>2</sub>MnO<sub>4-δ</sub> and CaMn<sub>2</sub>O<sub>4</sub> under CLC conditions [14]. In studies by Leion et al. [15] and Rydén et al. [16] a CaMnO<sub>3-δ</sub> particle doped with titanium has shown high oxygen release to inert atmosphere as well as high methane conversion. The titanium was incorporated in the crystal structure and is believed to stabilize the perovskite, to some extent preventing decomposition to Ca<sub>2</sub>MnO<sub>4-δ</sub> and CaMn<sub>2</sub>O<sub>4</sub>. Fossdal et al. [17] showed that these kinds of materials can be made using cheap Mn-ore and calcium hydroxide as raw materials.

In the materials used in the current study some of the manganese has been exchanged to magnesium or magnesium and titanium. The magnesium ion is however not of the right size to fit into the perovskite structure. In X-ray diffraction patterns the magnesium appeared as periclase (MgO) separate from the perovskite structure in the three materials. This phenomenon is more extensively discussed elsewhere [7, 18, 19].

**2.3. The Aim of This Study.** The oxygen carriers used in this study have previously been successfully examined in a batch reactor [18, 20, 21] with very positive results. The goal of the present study is to show that these formulations of CaMnO<sub>3-δ</sub> can be used as oxygen carriers also in continuous chemical-looping combustion/oxygen uncoupling. This means that the materials would need to be stable over many hours of fluidization and for hundreds or thousands of redox cycles.

### 3. Experimental

**3.1. Manufacturing of Oxygen-Carrier Particles.** All oxygen-carrier particles examined in this study were manufactured by VITO in Belgium by spray drying. The general procedure

TABLE 1: Material data.

Composition	Solids inventory [g]	Calcination temperature [°C]	Bulk density [ $\text{kg m}^{-3}$ ]
$\text{CaMn}_{0.8}\text{Mg}_{0.2}\text{O}_{3-\delta}$	250	1300	1100
$\text{CaMn}_{0.9}\text{Mg}_{0.1}\text{O}_{3-\delta}$	310	1300	1400
$\text{CaMn}_{0.775}\text{Mg}_{0.1}\text{Ti}_{0.125}\text{O}_{3-\delta}$	400	1350	1600

Reactor system

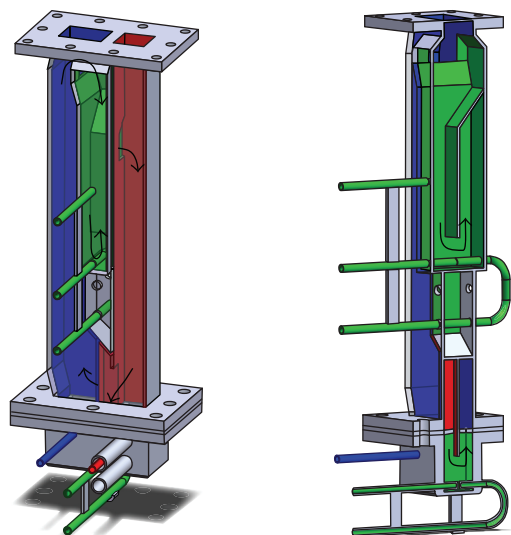


FIGURE 2: The reactor. Arrows are showing the flow direction of the particles. The air reactor is in blue, the fuel reactor is in red, and the downcomer and slot loop seals are shown in green. The pipes are the various gas inlets. In the slot and downcomer the bottom gas inlets consist of two separate pipes in order to distribute the gas evenly between the fuel reactor and air reactor side. In the downcomer one additional gas inlet sits at about half height and can be used in case of fluidization difficulties. Not shown in the image is the widened settling zone where the gas velocity is reduced so that particles fall back down into the reactor. Image courtesy of Patrick Moldenhauer.

was as follows. Powder mixtures of the raw materials were dispersed in deionized water containing organic additives, organic binder, and dispersants. The water-based suspension was continuously stirred with a propeller blade mixer while being pumped to a 2-fluid nozzle, positioned in the lower cone part of the spray-drier. Obtained particles were sieved and the fraction within the desired size range (diameter 106–212  $\mu\text{m}$ ) was separated from the rest of the spray-dried products. Sieved particles were then calcined in air at 1300 or 1350°C for 4 h. After calcination, the particles were sieved once more so that all particles used for experimental evaluation would be of well-defined size.

The compositions, calcination temperature, bulk density, and the solids inventory used during the experiments are shown in Table 1.

**3.2. Reactor System.** The reactor used for continuous testing has previously been used by Moldenhauer et al. [19, 22, 23] with a different fuel injection system and by Hallberg et al. [18]. A schematic picture of the reactor is shown in Figure 2. The reactor is designed to use a rather small amount of oxygen carriers with gaseous fuel. The amount of oxygen carrier required to operate the reactor depends on the density

of the oxygen carrier and is in the range 200–400 g. The inner dimensions of the AR are 25 mm  $\times$  42 mm in the base and decrease to 25 mm  $\times$  25 mm in the riser section. The inner dimension of the FR is 25 mm  $\times$  25 mm. The inner dimensions of the downcomer are 21 mm  $\times$  44 mm. The gas to the AR and FR enters wind boxes and is evenly distributed over the cross section by porous quartz plates. In the downcomer and bottom loop-seal (slot) gas enters through the pipes seen in Figure 2. These inlets are divided in two so that one inlet is on the FR side and the other is on the AR side. The gas is distributed through small holes drilled in the pipes directed downwards. The air flow in the AR is sufficiently high to throw the particles upwards to a wider settling zone (not shown in Figure 2) where they fall down. A fraction of the falling particles enters the downcomer loop seal. Via the return orifice they fall into the bubbling fuel reactor where they are reduced according to reaction (2) or (3). The height from the bottom of the FR to the return orifice is 165 mm. From the bottom of the FR the particles enter the slot loop seal and return to the AR where they are reoxidized according to reaction (1) and the loop is completed. To be able to operate the reactor at target temperature it is placed inside an electrically heated furnace since the scale is too small for autothermal operation. The oxygen depleted air from the AR passes through particle filter while the flue gases from the FR pass through a particle filter and water seal, before leaving the reactor system. Slip streams are extracted after both the air reactor and the fuel reactor and are taken to gas conditioning systems, in which each slip stream is further filtrated and water is condensed. Following the gas conditioning systems the concentrations of  $\text{O}_2$ ,  $\text{CO}_2$ ,  $\text{CO}$ , and  $\text{CH}_4$  are measured continuously using a combination of infrared and paramagnetic sensors.  $\text{N}_2$  and  $\text{H}_2$  from the FR are measured periodically by gas chromatography (GC). The gases in the AR and FR are somewhat diluted by the gas that fluidizes the slot. The gases are furthermore diluted with the gas from the downcomer when it leaves the AR/FR and dry gas concentrations measured are thus slightly lower than when leaving the reactor. For the experiments performed the flows used are  $F_{\text{AR}} = 4\text{--}7 \text{ L}_\text{N} \text{ min}^{-1}$  air or nitrogen diluted air,  $F_{\text{FR}} = 0.3\text{--}0.45 \text{ L}_\text{N} \text{ min}^{-1}$   $\text{CO}_2$  or natural gas,  $F_{\text{DOWNCOMER}} = 0.3 \text{ L}_\text{N} \text{ min}^{-1}$  each,  $F_{\text{SLOT}} = 0.1 \text{ L}_\text{N} \text{ min}^{-1}$  each; downcomer and slot were both fluidized with argon.

**3.3. Oxygen Uncoupling Experiments.** During the startup of experiments air was used to fluidize the reactor during heat-up to the desired temperature. After that the fuel reactor was fluidized with inert gas in order to study the particles ability to release oxygen. During the oxygen uncoupling experiments the AR was fluidized either with air or with air diluted with nitrogen to an oxygen concentration of 5%. The FR was fluidized with  $\text{CO}_2$  and the slot and downcomer

TABLE 2: List of experiments with natural gas.

Experiment	Operation (min)	$F_{FR}$ ( $L_N \text{ min}^{-1}$ )	$F_{AR}$ ( $L_N \text{ min}^{-1}$ )	$T_{FR}$ ( $^{\circ}\text{C}$ )
$\text{CaMn}_{0.8}\text{Mg}_{0.2}\text{O}_{3-\delta}$				
CLC <sub>I</sub>	70	0.15	6	900
CLC <sub>II</sub>	330	0.3	5-6	900
CLC <sub>III</sub>	190	0.4	6-7	900
CLC <sub>IV</sub>	290	0.3	6	700-950
$\text{CaMn}_{0.9}\text{Mg}_{0.1}\text{O}_{3-\delta}$				
CLC <sub>V</sub>	230	0.15-0.45	6	900
CLC <sub>VI</sub>	80	0.4	4-7	900
CLC <sub>VII</sub>	250	0.3	6	700-950
CLC <sub>VIII</sub>	400	0.3	6	900
$\text{CaMn}_{0.775}\text{Mg}_{0.1}\text{Ti}_{0.125}\text{O}_{3-\delta}$				
CLC <sub>IX</sub>	220	0.4	6	900
CLC <sub>X</sub>	430	0.3	6-7	900
CLC <sub>XI</sub>	430	0.35	6-7	900
CLC <sub>XII</sub>	960	0.4	6-7	900
CLC <sub>XIII</sub>	380	0.4	6-7	950

were fluidized with argon. The reason for examining two different oxidation cases is that the  $\delta$  factor in perovskite materials is known to be a function of oxygen partial pressure. Hence oxidation with air may provide an overestimation of the capability of the particles during practicable conditions. Oxidation with 5% oxygen was used to mimic the expected conditions at the top of the riser in a real-world unit operating with 20% excess air and constitutes a more realistic case.

There was some leakage of gas from the AR to the FR which affected the measured raw data slightly. The leakage was quantified with the GC by  $\text{N}_2$  measurement. The leakage was located to the top of the reactor, that is, over the fluidized bed. Hence the minor amounts of the oxygen that leaked from the AR are unlikely to have affected the oxygen release behavior. The measured oxygen concentration was therefore corrected with the following equation to disregard the leaked oxygen:

$$x_{\text{O}_2, \text{corrected FR}} = x_{\text{O}_2, \text{FR}} - \frac{x_{\text{N}_2, \text{FR}}}{(1 - x_{\text{O}_2, \text{AR}}) / x_{\text{O}_2, \text{AR}}}, \quad (6)$$

where  $x_{i,jR}$  is the measured molar fraction of species  $i$  exiting the  $j$  reactor. Since the  $\text{N}_2 : \text{O}_2$  ratio of the leaked gas is known the  $\text{N}_2$  in the fuel reactor is used to quantify how much  $\text{O}_2$  accompanied it. Basically, formula (6) just corrects oxygen release data for the small amounts of air leaking from the top of the air reactor to the top of the fuel reactor.

**3.4. Experiments with Natural Gas.** During the experiments with natural gas the AR was fluidized with air, the downcomer and slot with argon and the fuel reactor with natural gas (96% methane), or natural gas diluted with nitrogen. The temperature in the air reactor was 5–12 K higher than in the fuel reactor during fuel operation. The temperature difference varied with fuel flow and fuel conversion. A higher air reactor temperature will reduce the oxygen carrier degree of oxidation and consequently the fuel conversion. That problem would not occur in a commercial scale unit where heat extraction probably would be in the air reactor. In this study most focus is put on the relatively slow oxygen carrier reduction rather than oxidation. A consequence of this is that

when temperature is used it is the fuel reactor temperature, where the oxygen carrier reduction occurs. As a measure for combustion efficiency  $\text{CO}_2$  yield,  $\gamma$ , is used. The  $\text{CO}_2$  yield is defined as  $\text{CO}_2$  exiting the fuel reactor divided by all carbon containing species as

$$\gamma = \frac{x_{\text{CO}_2}}{x_{\text{CO}_2} + x_{\text{CO}} + x_{\text{CH}_4}}, \quad (7)$$

where  $x_i$  is the measured molar fraction of species  $i$ . This gives a value close to the combustion efficiency since the heating value of methane is similar to that of CO and corresponding amount of  $\text{H}_2$ . Possible leakage of carbon containing species from the FR to the AR is not taken into account.

## 4. Results

**4.1. Oxygen Uncoupling Experiments.** The temperature dependence of oxygen uncoupling is shown in Figures 3(a)–3(c). The figures show the oxygen concentration calculated according to (6) of the gas leaving the FR as a function of temperature in FR for two different oxygen partial pressures in the AR. As expected the oxygen release increased with temperature. This is most noticeable between 800 and 850 $^{\circ}\text{C}$ . The partial pressure of oxygen in the AR also had an effect on oxygen release. The  $\Delta\delta$  was obviously greater in the case with air for oxidation compared to the 5% oxygen case. When air was used for oxidation the measured oxygen concentration for gas leaving the air reactor was above 18%. Oxidation was therefore done with a large excess of oxygen. For the case when 5% oxygen was used to fluidize the air reactor the measured outgoing oxygen concentration was about 4%.  $\text{CaMn}_{0.8}\text{Mg}_{0.2}\text{O}_{3-\delta}$  gave the highest oxygen concentration in the fuel reactor. However, all three materials tested proved to be potent oxygen uncouplers. It can also be noted that the amount of leakage differed for the different particles but that is unlikely to have had any influence on the results.

**4.2. Experiments with Natural Gas.** The experimental conditions that were used are listed in Table 2. Operational parameters were adjusted in order to operate at full fuel

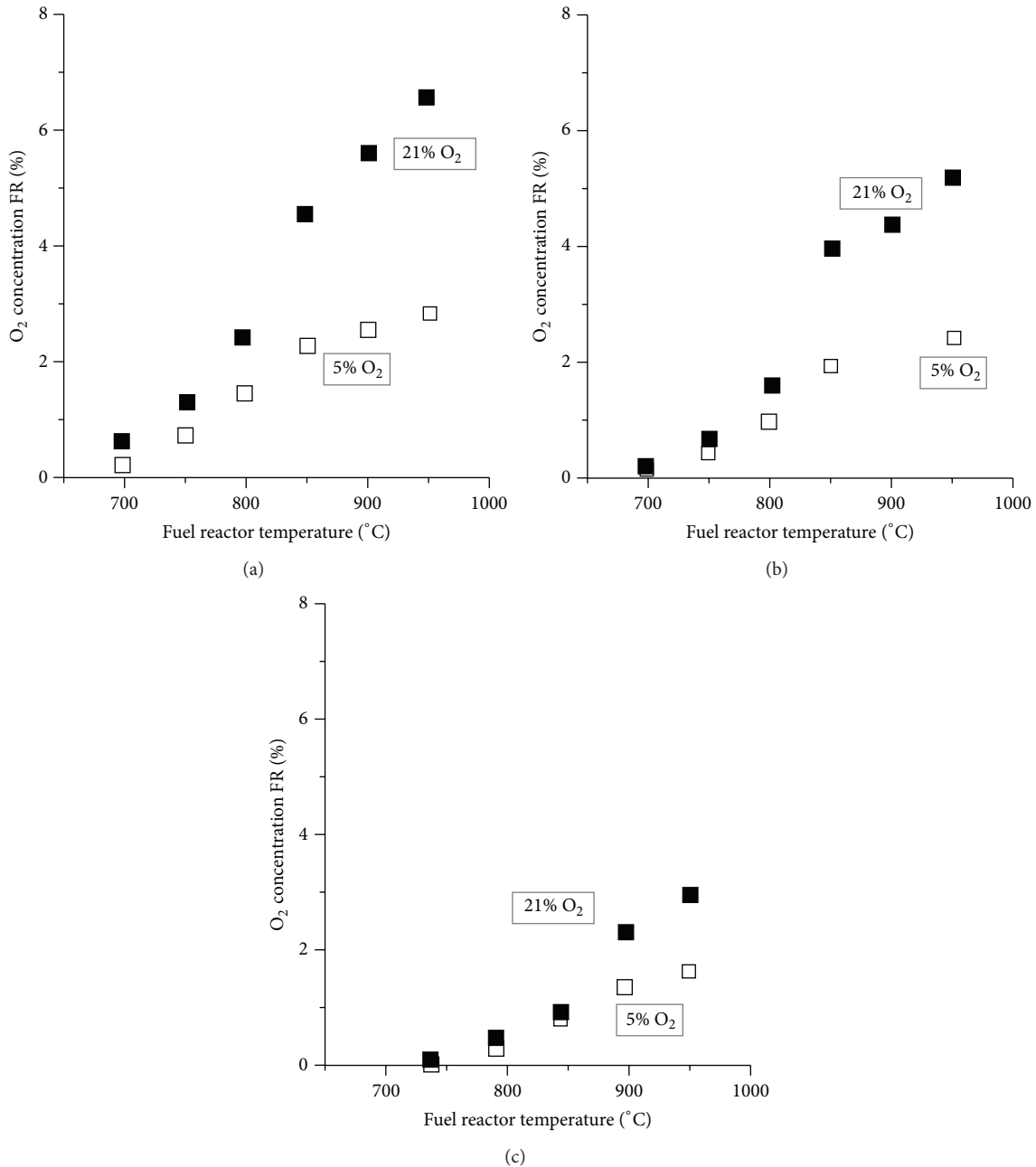


FIGURE 3: Effect of temperature and AR O<sub>2</sub> concentration on oxygen uncoupling for CaMn<sub>0.8</sub>Mg<sub>0.2</sub>O<sub>3-δ</sub> (a), CaMn<sub>0.9</sub>Mg<sub>0.1</sub>O<sub>3-δ</sub> (b), and CaMn<sub>0.775</sub>Mg<sub>0.1</sub>Ti<sub>0.125</sub>O<sub>3-δ</sub> (c). The oxygen concentration is corrected through (6).

conversion or close to it. Typically parameters (air flow, fuel flow, and temperature) were changed one at a time. For CLC<sub>I</sub> and CLC<sub>V</sub> fuels were cautiously introduced and for the fuel flow 0.15 L<sub>N</sub> min<sup>-1</sup> fuel was mixed with nitrogen. After the initial fuel introduction was successful fuel flow and air flow were tested at other levels as well. Figure 4 shows how the gas concentrations vary in the transition from CLC<sub>II</sub> to CLC<sub>III</sub>. By increasing fuel flow the fuel conversion goes from complete to incomplete. This is seen as the excess oxygen goes to zero and methane and carbon monoxide are >0. The increase in oxygen at 40 min is due to a leakage while controlling a filter. At experiments CLC<sub>IV</sub> and CLC<sub>VII</sub> a temperature stair

was tested. The temperature was gradually increased from 700 to 950°C.

The effect of temperature on the combustion efficiency can be seen in Figure 5. Here all three materials reach complete or almost complete fuel conversion. For these experiments the flows used are  $F_{AR} = 6 \text{ L}_N \text{ min}^{-1}$ ,  $F_{FR} = 0.3$ ,  $F_{DOWNCOMER} = 0.3 \text{ L}_N \text{ min}^{-1}$  each, and  $F_{SLOT} = 0.1 \text{ L}_N \text{ min}^{-1}$  each. In Figure 6 the combustion efficiency is shown as a function of fuel reactor particle load per fuel power. The fuel reactor inventory is estimated to be 26% of the total inventory based on measured bed heights after experiments termination. While particle inventory was held constant

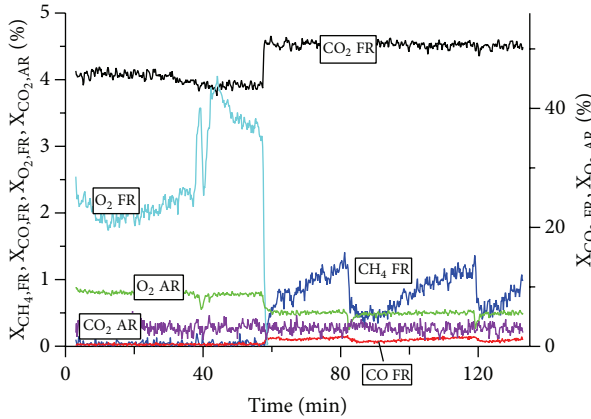


FIGURE 4: Measured dry gas composition for the transition from CLC<sub>II</sub> to CLC<sub>III</sub>. What can be seen is an instance when going from  $0.3 \text{ L}_N \text{ min}^{-1}$  fuel flow to  $0.4 \text{ L}_N \text{ min}^{-1}$ .  $F_{AR}$  is held at  $6 \text{ L}_N \text{ min}^{-1}$ . The operation goes from complete fuel conversion with excess oxygen to incomplete fuel conversion.

during experiments the parameter was changed by varying the fuel flow between  $0.3$  and  $0.45 \text{ L}_N \text{ min}^{-1}$ .

In general, the experiments with natural gas proceeded quite smoothly. There were some problems with  $\text{CaMn}_{0.8}\text{Mg}_{0.2}\text{O}_{3-\delta}$  and  $\text{CaMn}_{0.9}\text{Mg}_{0.1}\text{O}_{3-\delta}$  when the temperature was increased to  $950^\circ\text{C}$  though. At these temperatures the circulation of solids appears to have been negatively affected and the fuel conversion decreased. However, once fuel was switched to inert gas and the temperature reduced stable operation could be resumed.  $\text{CaMn}_{0.775}\text{Mg}_{0.1}\text{Ti}_{0.125}\text{O}_{3-\delta}$  on the other hand could be operated without problems at  $950^\circ\text{C}$ .

**4.3. Particle Integrity.** The tests with  $\text{CaMn}_{0.8}\text{Mg}_{0.2}\text{O}_{3-\delta}$  and  $\text{CaMn}_{0.9}\text{Mg}_{0.1}\text{O}_{3-\delta}$  unfortunately had to be aborted before schedule. The premature termination of experiments was due to significant particle leakage from the reactor system to the surroundings due to mechanical failure. Thus the attrition of  $\text{CaMn}_{0.8}\text{Mg}_{0.2}\text{O}_{3-\delta}$  and  $\text{CaMn}_{0.9}\text{Mg}_{0.1}\text{O}_{3-\delta}$  particles is estimated through what was found in filters after experiments. For  $\text{CaMn}_{0.8}\text{Mg}_{0.2}\text{O}_{3-\delta}$   $4.8 \text{ g}$  of fines was found in filters and water seal after operation which would correspond to  $0.13\%$  particles lost per hour of fuel operation. That number would be considerably smaller if operation at hot conditions with fluidization was used as base rather than operation with fuel. With  $\text{CaMn}_{0.9}\text{Mg}_{0.1}\text{O}_{3-\delta}$  not all the particles found in filters were fines ( $<45 \mu\text{m}$ ). If only fines are considered the loss of particles would be  $0.03\%$  per hour of fuel operation.

The experiments with  $\text{CaMn}_{0.775}\text{Mg}_{0.1}\text{Ti}_{0.125}\text{O}_{3-\delta}$  did not suffer any particle leakage. Hence a size distribution analysis could be performed without introducing systematic errors. Figure 7 shows particle size distribution for this material. The comparison is between the fresh particles added to the reactor and the used particles retrieved from the reactor. Only a small difference from the added and used particles can be seen which indicates that the particles could withstand attrition

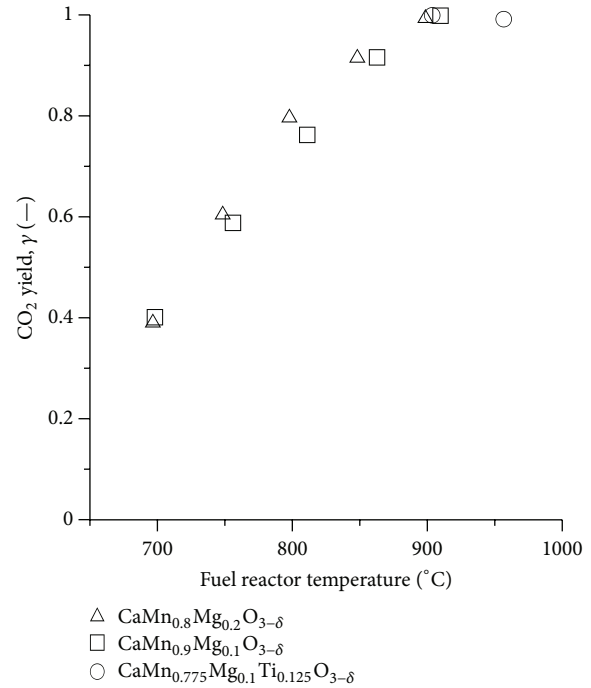


FIGURE 5: Effect of temperature on combustion efficiency for the used materials. The plotted values are averages for 15 min operation at each temperature.  $F_{FR,ng}$  was  $0.3 \text{ L}_N \text{ min}^{-1}$  except for the point at  $T = 950^\circ\text{C}$  where  $F_{FR,ng}$  was  $0.4 \text{ L}_N \text{ min}^{-1}$ .  $F_{AR,air}$  was  $6 \text{ L}_N \text{ min}^{-1}$ .

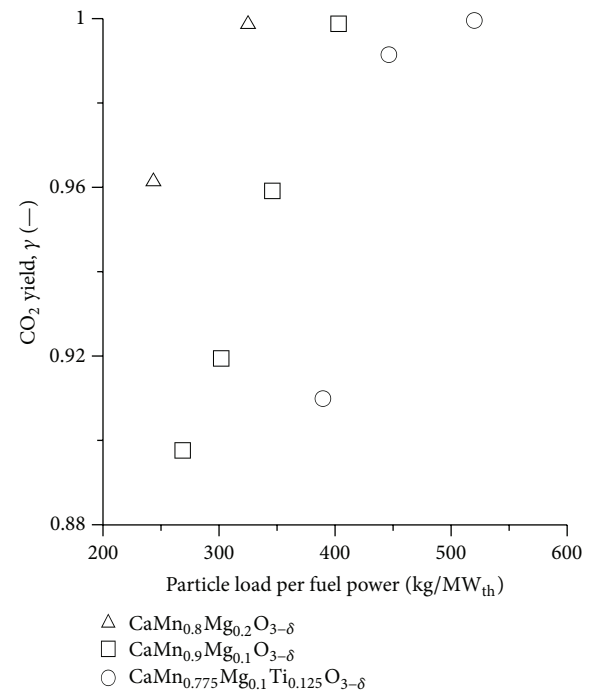


FIGURE 6:  $\text{CO}_2$  yield as a function of solids inventory in FR per fuel power. The load was changed with the volumetric fuel flow (from  $0.3$  to  $0.45 \text{ L}_N \text{ min}^{-1}$ ) and it was assumed that  $26\%$  of the total inventory was located in the FR. Air flow was  $6 \text{ L}_N \text{ min}^{-1}$  and temperature was  $900^\circ\text{C}$ . Each data point is an average of 15 minutes of operation.

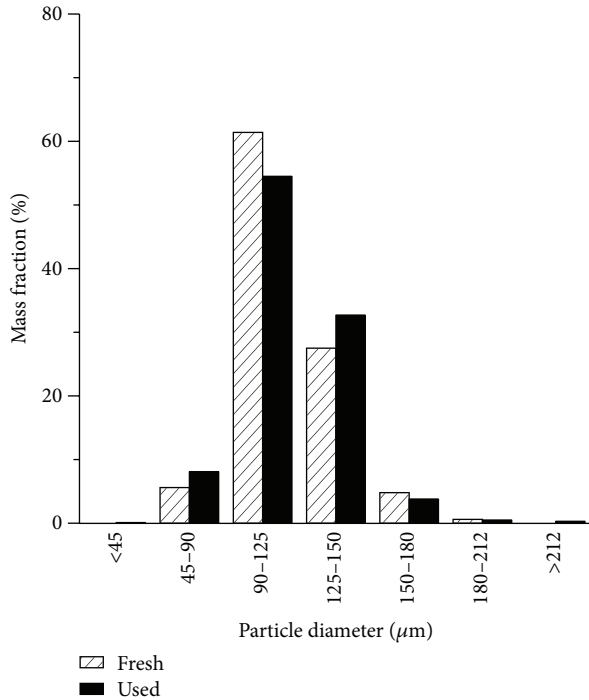


FIGURE 7: Particle size distribution for  $\text{CaMn}_{0.775}\text{Mg}_{0.1}\text{Ti}_{0.125}\text{O}_{3-\delta}$ , comparison between fresh particles added to reactor and the retrieved used ones.

well. Using the same measure as above the loss of particles was 0.08% per hour of fuel operation.

**4.4. Effects of Operation.** It was noticed during the operation with  $\text{CaMn}_{0.775}\text{Mg}_{0.1}\text{Ti}_{0.125}\text{O}_{3-\delta}$  that the reactivity seemed to decrease slightly as a function of operation time. This phenomenon was examined by testing the reactivity of the used particles in a small batch reactor. The experiments were performed using the same equipment and methodology as Hallberg et al. [18] did in a previous study. Thus the reactivity of fresh particles and the particles that had been used in the 300 W unit could be examined, isolating possible sources of error such as rate of solids circulation. The comparison is presented in Figure 8, in which data for  $\text{CaMn}_{0.9}\text{Mg}_{0.1}\text{O}_{3-\delta}$  also have been included. A reduced  $\text{CO}_2$  yield for used oxygen carrier particles can be seen for both materials. The effect on  $\text{CaMn}_{0.775}\text{Mg}_{0.1}\text{Ti}_{0.125}\text{O}_{3-\delta}$  is considerably larger than for  $\text{CaMn}_{0.9}\text{Mg}_{0.1}\text{O}_{3-\delta}$  though. A possible explanation for the larger impact of operation on this material is operating time.  $\text{CaMn}_{0.9}\text{Mg}_{0.1}\text{O}_{3-\delta}$  was tested for 16 h with fuel in the continuous unit whereas  $\text{CaMn}_{0.775}\text{Mg}_{0.1}\text{Ti}_{0.125}\text{O}_{3-\delta}$  was tested for more than 40 h. Oxygen release to inert atmosphere was also examined in batch reactor but the difference between used and fresh particles was very small, as shown in Figure 9. In an attempt to explain the decrease in reactivity the particles were examined by X-ray powder diffraction. For  $\text{CaMn}_{0.9}\text{Mg}_{0.1}\text{O}_{3-\delta}$  an increase in the marokite ( $\text{CaMn}_2\text{O}_4$ ) peaks was detected. A comparison of the fresh and used

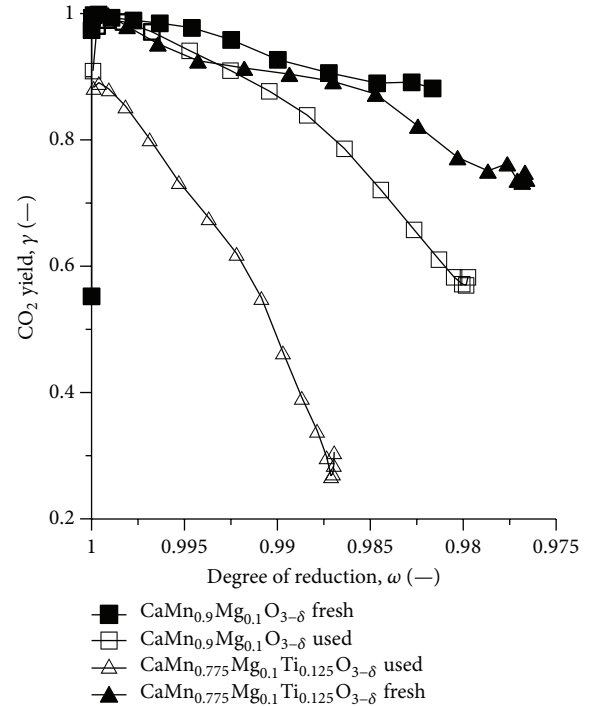


FIGURE 8:  $\text{CO}_2$  yield as a function of degree of reduction. Results from reduction with methane in quartz batch reactor. Fresh particles are compared with materials used in the 300 W unit. These results are performed at  $950^\circ\text{C}$ .

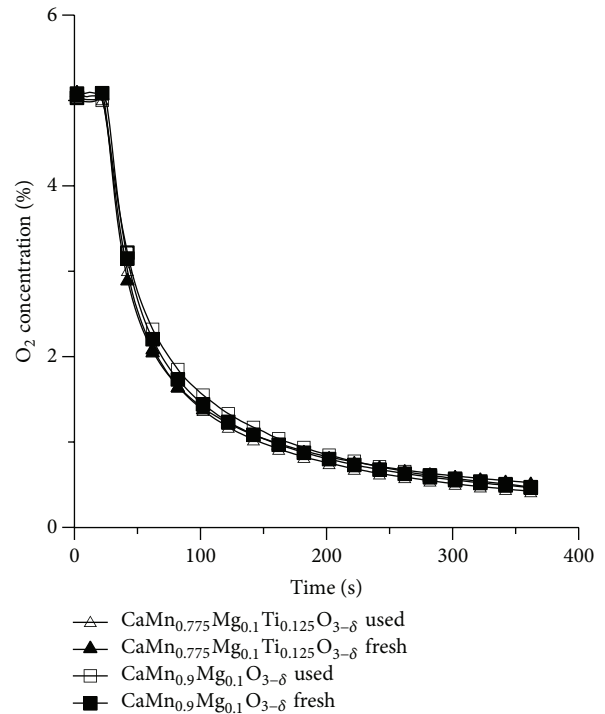


FIGURE 9: Outgoing oxygen concentration during batch experiments. The fluidizing gas is changed from 5% oxygen in nitrogen to 100% nitrogen at time 0. The 20 s delay is the time it takes for gas to reach gas analyzer. Fresh particles are compared to particles which have been used in the 300 W unit.

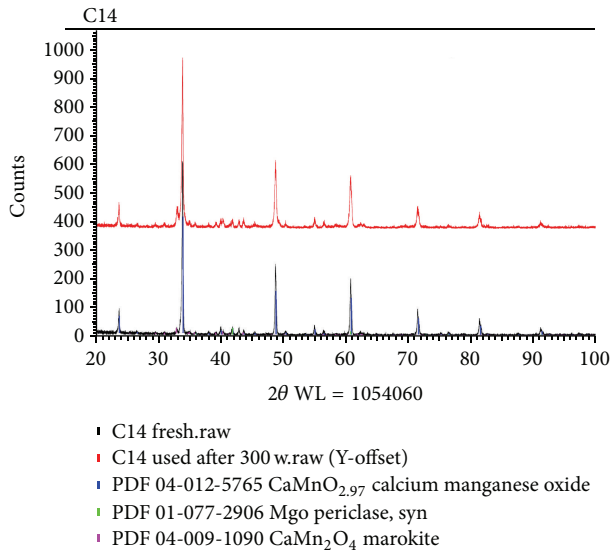


FIGURE 10: X-ray diffraction pattern including fresh and used  $\text{CaMn}_{0.9}\text{Mg}_{0.1}\text{O}_{3-\delta}$ . An increase in the  $\text{CaMn}_2\text{O}_4$  peaks (in magenta at 31, 33, 39, and 44) can be seen in the used particles.

particles is shown in Figure 10. The decomposition was not detected for  $\text{CaMn}_{0.775}\text{Mg}_{0.1}\text{Ti}_{0.125}\text{O}_{3-\delta}$ .

## 5. Discussion and Conclusions

The purpose of this work is to investigate materials other than nickel oxide materials, representing the state of art for chemical-looping combustion of gaseous fuels. The results are highly encouraging as follows:

- (i) the materials studied are able to reach complete gas conversion in contrast to nickel oxide materials which are limited to 98–99% conversion;
- (ii) the materials studied are composed of raw materials very much cheaper than nickel oxide;
- (iii) the materials studied are not associated with significant risks for health and environment in contrast to nickel;
- (iv) the materials seem to have low attrition rates.

The experimental campaign was thus, despite a few minor setbacks, a success. In addition to the points made above:

- (i) all three tested materials released oxygen to inert atmosphere;
- (ii) for  $\text{CaMn}_{0.8}\text{Mg}_{0.2}\text{O}_{3-\delta}$  a FR particle inventory of 240 kg/MW<sub>th</sub> was needed for complete natural gas conversion at 900°C and for  $\text{CaMn}_{0.9}\text{Mg}_{0.1}\text{O}_{3-\delta}$  the FR particle inventory needed was 400 kg/MW<sub>th</sub>.  $\text{CaMn}_{0.775}\text{Mg}_{0.1}\text{Ti}_{0.125}\text{O}_{3-\delta}$  reached complete conversion at a FR particle inventory of 450 kg/MW<sub>th</sub> for 900°C and 390 kg/MW<sub>th</sub> for 950°C.

## Notations

- AR: Air reactor  
 FR: Fuel reactor  
 $F_i$ : Volume flow in inlet  $i$   
 $T_{jR}$ : Temperature in reactor  $j$   
 $x_i$ : Molar fraction of species  $i$   
 $x_{i,jR}$ : Molar fraction of species  $i$  in reactor  $j$   
 $\gamma$ :  $\text{CO}_2$ -yield  
 $\delta$ : Oxygen deficiency in perovskite structure  
 $\omega$ : Oxygen carrier degree of oxidation.

## Conflict of Interests

The authors declare that there is no conflict of interests regarding the publication of this paper.

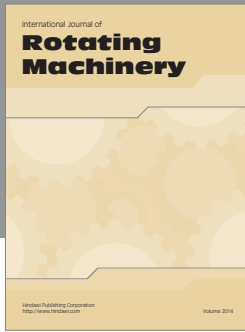
## Acknowledgment

This research has received funding from the European Union Seventh Framework Program (FP7/2007–2013) via Grant agreement no. 241401.

## References

- [1] Copenhagen Accord, *U.N. Framework Convention on Climate Change*, 2009.
- [2] M. E. Boot-Handford, J. C. Abanades, E. J. Anthony et al., “Carbon capture and storage update,” *Energy & Environmental Science*, vol. 7, pp. 130–189, 2014.
- [3] P. Kolbitsch, J. Bolh ar-Nordenkampf, T. Pr oll, and H. Hofbauer, “Operating experience with chemical looping combustion in a 120 kW dual circulating fluidized bed (DCFB) unit,” *International Journal of Greenhouse Gas Control*, vol. 4, no. 2, pp. 180–185, 2010.
- [4] C. R. Forero, P. Gay an, L. F. de Diego, A. Abad, F. Garc a-Labiano, and J. Ad anez, “Syngas combustion in a 500 Wth chemical-looping combustion system using an impregnated Cu-based oxygen carrier,” *Fuel Processing Technology*, vol. 90, no. 12, pp. 1471–1479, 2009.
- [5] H. R. Kim, D. Wang, L. Zeng et al., “Coal direct chemical looping combustion process: design and operation of a 25-kW<sub>th</sub> sub-pilot unit,” *Fuel*, vol. 108, no. 0, pp. 370–384, 2013.
- [6] C. Linderholm, T. Mattisson, and A. Lyngfelt, “Long-term integrity testing of spray-dried particles in a 10-kW chemical-looping combustor using natural gas as fuel,” *Fuel*, vol. 88, no. 11, pp. 2083–2096, 2009.
- [7] L.-S. Fan, *Chemical Looping Systems for Fossil Energy Conversion*, John Wiley & Sons, 2010.
- [8] J. Adanez, A. Abad, F. Garcia-Labiano, P. Gayan, and L. F. De Diego, “Progress in chemical-looping combustion and reforming technologies,” *Progress in Energy and Combustion Science*, vol. 38, no. 2, pp. 215–282, 2012.
- [9] A. Lyngfelt, “Chemical-looping combustion of solid fuels—status of development,” *Applied Energy*, vol. 113, pp. 1869–1873, 2014.
- [10] M. Ishida and H. Jin, “A novel chemical-looping combustor without NO<sub>x</sub> formation,” *Industrial and Engineering Chemistry Research*, vol. 35, no. 7, pp. 2469–2472, 1996.

- [11] T. Mattisson, A. Lyngfelt, and H. Leion, "Chemical-looping with oxygen uncoupling for combustion of solid fuels," *International Journal of Greenhouse Gas Control*, vol. 3, no. 1, pp. 11–19, 2009.
- [12] M. Rydén, H. Leion, T. Mattisson, and A. Lyngfelt, "Combined oxides as oxygen-carrier material for chemical-looping with oxygen uncoupling," *Applied Energy*, vol. 113, pp. 1924–1932, 2014.
- [13] C. Li, K. C. K. Soh, and P. Wu, "Formability of ABO<sub>3</sub> perovskites," *Journal of Alloys and Compounds*, vol. 372, no. 1–2, pp. 40–48, 2004.
- [14] E. Bakken, T. Norby, and S. Stølen, "Nonstoichiometry and reductive decomposition of CaMnO<sub>3-δ</sub>," *Solid State Ionics*, vol. 176, no. 1–2, pp. 217–223, 2004.
- [15] H. Leion, Y. Larring, E. Bakken, R. Bredesen, T. Mattisson, and A. Lyngfelt, "Use of CaMn<sub>0.875</sub>Ti<sub>0.125</sub>O<sub>3</sub> as oxygen carrier in chemical-looping with oxygen uncoupling," *Energy and Fuels*, vol. 23, no. 10, pp. 5276–5283, 2009.
- [16] M. Rydén, A. Lyngfelt, and T. Mattisson, "CaMn<sub>0.875</sub>Ti<sub>0.125</sub>O<sub>3</sub> as oxygen carrier for chemical-looping combustion with oxygen uncoupling (CLOU)—experiments in a continuously operating fluidized-bed reactor system," *International Journal of Greenhouse Gas Control*, vol. 5, no. 2, pp. 356–366, 2011.
- [17] A. Fossdal, E. Bakken, B. A. Øye et al., "Study of inexpensive oxygen carriers for chemical looping combustion," *International Journal of Greenhouse Gas Control*, vol. 5, no. 3, pp. 483–488, 2011.
- [18] P. Hallberg, D. Jing, M. Rydén, T. Mattisson, and A. Lyngfelt, "Chemical looping combustion and chemical looping with oxygen uncoupling experiments in a batch reactor using spray-dried CaMn<sub>1-x</sub>M<sub>x</sub>O<sub>3-δ</sub> (M = Ti, Fe, Mg) particles as oxygen carriers," *Energy and Fuels*, vol. 27, no. 3, pp. 1473–1481, 2013.
- [19] M. Rydén and M. Arjmand, "Continuous hydrogen production via the steam-iron reaction by chemical looping in a circulating fluidized-bed reactor," *International Journal of Hydrogen Energy*, vol. 37, no. 6, pp. 4843–4854, 2012.
- [20] D. Jing, T. Mattisson, M. Ryden et al., "Innovative oxygen carrier materials for chemical-looping combustion," *Energy Procedia*, vol. 37, pp. 645–653, 2013.
- [21] D. Jing, T. Mattisson, H. Leion, M. Rydén, and A. Lyngfelt, "Examination of perovskite structure CaMnO<sub>3-δ</sub> with MgO addition as oxygen carrier for chemical looping with oxygen uncoupling using methane and syngas," *International Journal of Chemical Engineering*, vol. 2013, Article ID 679560, 16 pages, 2013.
- [22] P. Moldenhauer, M. Rydén, T. Mattisson, and A. Lyngfelt, "Chemical-looping combustion and chemical-looping reforming of kerosene in a circulating fluidized-bed 300 W laboratory reactor," *International Journal of Greenhouse Gas Control*, vol. 9, pp. 1–9, 2012.
- [23] P. Moldenhauer, M. Rydén, T. Mattisson, M. Younes, and A. Lyngfelt, "The use of ilmenite as oxygen carrier with kerosene in a 300 W CLC laboratory reactor with continuous circulation," *Applied Energy*, vol. 113, pp. 1846–1854, 2014.



# Hindawi

Submit your manuscripts at  
<http://www.hindawi.com>

